Calibration of a 2D Scanning Radar and a 3D Lidar

Jan M. Rotter and Bernardo Wagner[a]
Real Time Systems Group, Leibniz University of Hanover, Appelstraße 9a, 30167 Hanover, Germany

Keywords: Mobile Robotics, 2D Scanning Radar, 3D Lidar, Target-less Calibration, Search and Rescue Robotics.

Abstract: In search and rescue applications, mobile robots have to be equipped with robust sensors that provide data under rough environmental conditions. One such sensor technology is radar which is robust against low-visibility conditions. As a single sensor modality, radar data is hard to interpret which is why other modalities such as lidar or cameras are used to get a more detailed representation of the environment. A key to successful sensor fusion is an extrinsically and intrinsically calibrated sensor setup. In this paper, a target-less calibration method for scanning radar and lidar using geometric features in the environment is presented. It is shown that this method is well-suited for in-field use in a search and rescue application. The method is evaluated in a variety of use-case relevant test scenarios and it is demonstrated that the calibration results are accurate enough for the target application. To validate the results, the proposed method is compared to a target-based state-of-the-art calibration method showing equivalent performance without the need for specially designed targets.

1 INTRODUCTION

A civil use-case of autonomous robots is search and rescue (SAR) (Kim et al., 2015) (Fritsche et al., 2017) (Fan et al., 2019). In disaster situations, first responders need to act as quickly as possible while protecting their own life. SAR robots provide a means to get an overview of a situation or to search for survivors in places that are not reachable by human helpers. Usually, disaster sites are considered harsh and challenging environments. They can be covered in dust or smoke with objects lying or hanging around and blocking the path of an autonomous robot. Therefore, SAR robots are equipped with robust sensor modalities. To recognize smaller objects, a high-resolution lidar or camera could be used. But these modalities lose precision in smoke or dust since a visual line of sight to the target is needed. To ensure basic operation, radar can be used as an additional sensor that is robust against these disturbances but is not as precise as visual sensor modalities (Fritsche et al., 2017). To maximize information value, sensor readings from multiple modalities can be fused (Fritsche et al., 2016). Essential for sensor fusion is an extrinsic and intrinsic calibration providing translation and rotation between the sensors as well as any scaling or offset parameters inherent to a specific sensor. There exist multiple methods to calibrate a sensor setup. Manual measurement can only provide an approximation since in most cases the sensor's origin is unknown. Also, intrinsic parameters can be hard or even impossible to measure. External measurement tools like laser trackers or optical tracking systems provide higher precision in determining the extrinsic parameters while the direct extraction of intrinsic parameters remains problematic. To find an extrinsic and also intrinsic set of calibration parameters, corresponding sensor readings between two sensors can be used. These methods can be divided into target-based and target-less methods. The target-based calibration uses carefully designed targets that are easy

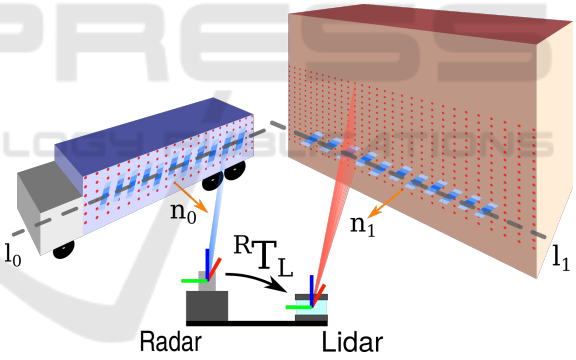

Figure 1: Schematic of the proposed in-field calibration method for search and rescue robots.

[a] https://orcid.org/0000-0001-5900-0935

Rotter, J. and Wagner, B.
Calibration of a 2D Scanning Radar and a 3D Lidar.
DOI: 10.5220/0011140900003271
In *Proceedings of the 19th International Conference on Informatics in Control, Automation and Robotics (ICINCO 2022)*, pages 377-384
ISBN: 978-989-758-585-2; ISSN: 2184-2809

to detect in all sensor modalities. Time-synchronized detections are used as correspondences and the distances between detections are minimized over all correspondences. In contrast, target-less methods only use corresponding features detected in the environment. In SAR applications only manual or target-less calibration can be used. Although target-based methods could be used in the field, they are impractical due to the calibration targets that require additional packaging space. Moreover, target-based methods usually take a longer time when the calibration target has to be moved to several different positions. External calibration tools can only be used when the sensor setup is never changed. This cannot be ensured since equipment may be disassembled for minimized packaging space. In this paper, an efficient target-less calibration method for 2D scanning radar and 3D lidar is presented. In contrast to the few other target-less approaches to this problem, calibrating the intrinsic offset parameter that exists in most scanning radar sensors is additionally considered. As calibration features, geometric primitives like planes and lines that can be found in a structured or semi-structured environment are used.

2 RELATED WORKS

Radar as a sensor modality in mobile robotics has recently become more popular. Over time various calibration methods for different sensor setups have been developed. The applied techniques mainly use target-based methods although a few target-less approaches exist.

2.1 Target-based Methods

Sugimoto et al. determine the extrinsic parameters between a monocular camera and a static 2D radar. A single corner reflector is used as a calibration target which is moved perpendicular to the radar plane. Local maxima in the radar measurements are considered to be crossing points of the reflector and radar plane where a corresponding camera measurement is recorded. All corresponding measurements are used in a least-squares estimation to calculate the extrinsic calibration (Sugimoto et al., 2004). Wang et al. use a similar approach but with a sheet of metal as a calibration target which is detected in both camera and radar. To filter the measurements a clustering algorithm is applied to the target detections (Wang et al., 2011). El Natour et al. are the first to relax the zero-elevation assumption of radar measurements. They take into account that not every radar measurement is located in the center of the measurement cone. Therefore, a 3D point detected in both camera and radar is modeled as the intersection of the light ray passing through this point and the camera center with a sphere centered at the radar center. The sensor setup is moved around multiple corner targets and the trajectory of the movement is used in the optimization process (El Natour et al., 2015). Peršić et al. present a calibration target that can be used for camera, lidar, and radar calibration simultaneously based on a corner reflector behind a triangular-shaped styrofoam plane with a checkerboard pattern. For the extrinsic calibration between lidar and radar, the radar cross-section (RCS) is used to estimate the elevation angle of the reflected radar signals and to refine the Z-axis parameter (Peršić et al., 2017) (Peršić et al., 2019). Domhof et al. use a target design consisting of a styrofoam plane with four circular holes and a corner reflector in the center for camera, lidar, and radar calibration. In contrast to El Natour et al., radar detections are considered to lie on a 2D plane. In their experiments, it is shown that the Root Mean Square Error (RMSE) is approximately 2 cm for the lidar-to-radar calibration and 2.5 cm for the camera-to-radar calibration (Domhof et al., 2019). In a follow-up work, experiments to evaluate different calibration constraints, as well as relative and absolute calibration results are added (Domhof et al., 2021).

2.2 Target-less Methods

Schöller et al. introduce a data-driven method to calibrate a camera-radar-system without calibration targets. They train two neural networks in a boosting-inspired algorithm to estimate the rotational calibration parameters. The euclidean distance between the estimated and true quaternion is used as loss function (Scholler et al., 2019). To calibrate a system of multiple laser scanners and automotive radar sensors, Heng uses a previously built map to first calibrate the laser scanners to each other. In a second step, the point-to-plane distance of the radar target detections to the mapped points is minimized (Heng, 2020). A different approach is used by Wise et al. In their work, velocity vectors from a camera-radar setup are extracted from the sensor data for each sensor individually which are used to estimate the extrinsic parameters (Wise et al., 2021). Peršić et al. also present a target-less calibration method that can be used as a decalibration detection as well. In every sensor modality, features are detected and tracked individually to obtain the sensor's trajectory. An association algorithm is used to find differences between the different sensor paths. If deviations are detected, a graph-based calibration towards one anchoring sensor is per-

formed. The authors state that the method is limited to rotational calibration and decalibration detection only (Peršić et al., 2021).

2.3 Contribution

In this paper, a target-less calibration method based on geometric primitives is presented. It is specially designed for in-field use in the SAR domain. Unlike all previously mentioned works, a scanning radar is employed instead of fixed *n*-channel sensor modules. Additionally, the internal offset parameter which is introduced by the rotating mirror as well as electrical signal delays is optimized. Raw range profiles are used instead of previously extracted target detections common to commercial automotive radar modules. Feature detection is applied to both radar and lidar to extract geometric primitives in both modalities. The calibration is modeled as a graph optimization problem. To ensure a good calibration quality, filtering methods to collect features with a greater variety via azimuth and elevation binning are applied. Evaluation is provided to analyze the absolute calibration error which is compared to the results of the target-based method by Peršić et al.

3 METHODOLOGY

The calibration method consists of a three-step preprocessing, matching, and optimization pipeline. First, raw sensor data is filtered to extract the relevant points from the radar and lidar respectively. Second, features from different sensor modalities are assigned to each other to build the constraints used in the optimization. Last, the set of constraints is filtered to keep informative matches and graph optimization is used to estimate the parameters.

3.1 Assumptions

Both sensors have to be synchronized in time. This is necessary to assign a corresponding lidar scan to each radar scan. Also, velocities of sensor movements are assumed to be slow enough that motion correction can be omitted. Finally, a set of initial calibration parameters is needed to transform the points into one common coordinate frame. The method mainly applies to FMCW radar sensors with a rotating mirror, although it may be used with other radar sensors as well for example by constraining the distance offset parameter to zero. For the proposed method the radar data consists of uncalibrated range profiles of which the range resolution has to be known in advance. The resolution can be calculated from the bandwidth and the analog-digital-converter parameters of the sensor.

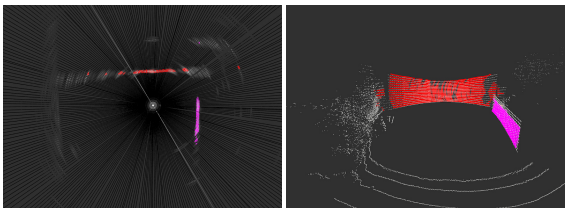

(a) Radar scan. (b) Lidar scan.

Figure 2: Visualization of processed sensor data from an outdoor data set. *(a)*: Raw radar data (black/white) and detected lines (colored). *(b)*: Raw lidar data (white) and detected planes (colored). A photo of the scene can be seen in Figure 6f.

3.2 Preprocessing

The first step is to process the data of each sensor individually to extract the features used in the matching and optimization step. Starting with the radar sensor, each scan is filtered by a standard CA-CFAR filter (Keel, 2010) that has to be tuned manually to the sensor's dynamic range. This removes noise and most of the clutter from the radar signal so that only potential target points including multi-path reflections remain. Since valid target points behind walls or other obstacles would not be seen by the lidar, all radar target detections behind the first one are removed. This also reduces multi-path reflections to a minimum. Then a RANSAC model (Fischler and Bolles, 1981) is used to search for lines in the radar target points which are highly likely to be found in structured and semi-structured environments. The distance for a point to be considered an inlier to a line is set to a more tolerant value compared to what would be necessary for lidar points since the results of the CFAR filter are not as accurate as lidar data. This results in a set of line parameters and their corresponding inlier points. Figure 2a shows the raw radar sensor data (black & white) as well as the extracted line points (colored).

The lidar data is first processed by a statistical outlier filter to remove very small objects or erroneous measurements. After using a voxel grid filter, a range image of the point cloud is created. To find large homogeneous regions which are typical for planes in structured environments, the magnitude of the gradients in the range image is calculated and filtered by a threshold. The remaining point locations involve only limited changes in the range between neighboring points. To refine the regions, a distance transform is applied and all points in the border areas of the homogeneous regions are removed. The range image is

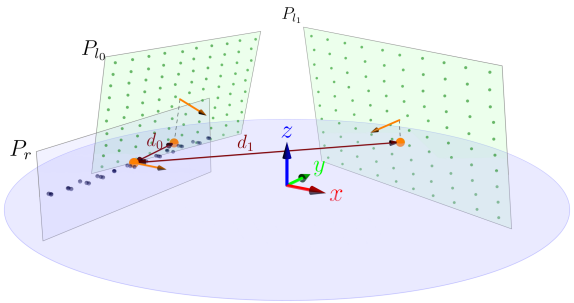

Figure 3: Matching of detected lidar planes P_{l_i} to a radar line represented by a helper plane P_r.

then transformed back into a point cloud. To achieve a more robust plane fitting, ground segmentation is performed and the potential ground plane is removed. In this reduced lidar cloud, planes that are perpendicular to the radar plane up to an angle ε are extracted. This angle should be chosen big enough, for example, $\varepsilon = 45°$, so that also tilted planes from the environment intersecting with the radar plane are recognized. A RANSAC model is used for the plane extraction, too. The result of the plane search can be seen in Figure 2b where raw lidar points are white and the identified planes are indicated by different colors.

3.3 Matching

Processing both sensor modalities results in a set of line parameters and corresponding radar target points as well as a set of plane parameters with their corresponding lidar points. To find matches between these two sets, first, the parameters of a helper plane P_r perpendicular to the radar measurement plane are calculated for each detected radar line. For each lidar plane P_{l_i}, the normal vector is projected onto the radar measurement plane. Then the intersection point between the projected normal vector and the detected lidar plane is determined. A correspondence is formed by a plane-line pair where the distance d_i between the normal intersection point of the radar helper plane and the intersection point calculated for the lidar plane is minimal. A visualization of the matching step is given in figure 3. This ensures that direction, as well as distance, are taken into account and also that heavily tilted lidar planes can be matched to a radar line detection. To ensure proper distribution of correspondences over the whole sensing area, all correspondences are assigned to an azimuth and elevation bin based on the respective angles of the lidar plane's normal vector. Correspondence samples are collected until at least N samples are recorded for every bin combination.

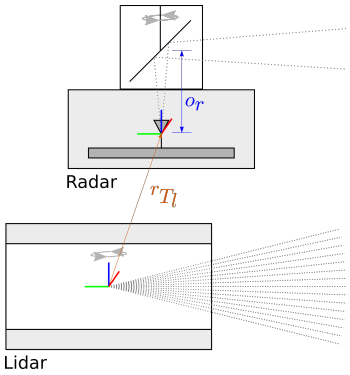

Figure 4: System overview.

3.4 Optimization

Scanning radars use a spinning mirror above the transmitter/receiver antenna. This leads to a distance offset in the raw sensor data o_r as depicted in Figure 4. The internal signal paths between the signal generator, antenna, and the A/D-converter increase this distance offset. Therefore, additionally to the extrinsic calibration parameters, the distance offset is optimized. The optimization problem is modeled as a graph with only one optimizable vertex v_0 which holds the calibration parameters using the *g2o*-framework (Kummerle et al., 2011). For every line-to-plane-correspondence, the lidar plane parameters are inserted as non-optimizable vertices v_k. For every radar line point, an edge defining the measurement of the radar error as

$$e(n_l, p_r, {}^rT_l, o_r) = n_l * {}^rT_l{}^{-1} * \left(p_r + o_r * \frac{p_r}{\|p_r\|} \right) \quad (1)$$

is inserted between the parameter vertex v_0 and the correspondence vertex v_k effectively minimizing the point-to-plane distance. Here n_l is the plane normal of the laser plane, p_r is the point from the corresponding radar line, ${}^rT_l$ is the 3D transformation matrix from the radar to the lidar coordinate frame and o_r is the intrinsic radar offset parameter.

The uncertainty of the radar measurements which originates from two sources is also modeled. First, in FMCW radar the continuous signals are sampled and discretized by the A/D converter. This discretization through the sampling rate into fixed-sized bins defines the range resolution and is used as the range uncertainty. Second, the expansion of the transmitted radar signal depends highly on the antenna used in the sensor module. Antennas form the shape of the main and side lobes of the radar beam. The field of view of the radar beam is defined as the -3 dB range of the main lobe and can be modeled as a cone. The uncertainty of the azimuth and elevation angle is therefore

set to the size of the field of view. At 0°azimuth, this results in a covariance matrix of

$$\Sigma_0(d) = \begin{pmatrix} s_{bin}^2 & 0 & 0 \\ 0 & (d\tan\alpha_{fov})^2 & 0 \\ 0 & 0 & (d\tan\alpha_{fov})^2 \end{pmatrix} \quad (2)$$

with range bin size s_{bin}, range measurement $d = \|p_r\|$ and field of view angle α_{fov}. For other azimuth or in the general case elevation angles the respective rotation has to be applied.

4 EXPERIMENTS

To validate the method and to compare it to methods from the state-of-the-art, multiple experiments are conducted using a *Velodyne VLP-16 Puck* as a laser scanner and two different scanning radars *(Navtech CIR204, Indurad iSDR-C)*. The laser scanner uses 16 rays in its vertical field of view of 30°at a horizontal resolution of 0.3°. The Navtech radar has a beam opening angle of 1.8°, a horizontal resolution of 0.9°, and a range resolution of 0.06 m, whereas the Indurad radar has a beam opening angle of about 3°at a similar horizontal resolution and a range resolution of 0.04 m. All sensors have a horizontal field of view of 360°. Three different sensor setups which are shown in Figure 5 are used. In the first setup *(a)* the *Indurad* radar and the *Velodyne* lidar are mounted on top of each other on a handheld sensor frame to provide a better motion radius and to verify that the method can provide a reasonably good lidar-to-radar calibration. For a second experiment, the same sensor setup is placed underneath a UAV platform *(b)* that could be used in a search and rescue scenario. The UAV is moved and tilted manually with two persons to show that the method works in a real-world scenario and can speed up the calibration process in an emergency situation. The last setup *(c)* is built onto an UGV platform using the *Navtech* radar along with the *Velodyne* lidar. In this setup, a greater distance between the sensors is chosen to find out how the method deals with fewer constraints through movement and rotation. For all setups, ground truth for the extrinsic 6-DOF parameter set is measured. The ground truth information for the first two setups is extracted from CAD models. To obtain ground truth parameters for the third setup, an optical tracking system is used to measure translation and rotation between the sensors on the mobile platform. To determine the internal offset parameter, the distance between the center of the radome and a single corner reflector is first measured by using the tracking system and then by detecting the reflector in the radar scan. The difference between both measurements is used as ground truth offset. All ground truth

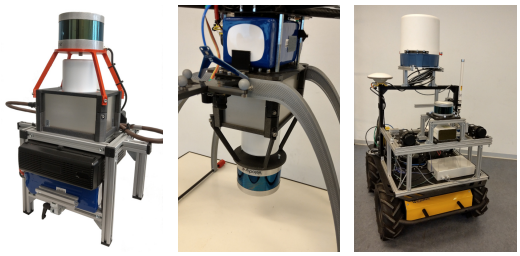

(a) (b) (c)

Figure 5: Sensor setups used in the experiments. Handheld sensor box *(a)*, UAV *(b)* and *(c)* UGV mounted setups.

(a) (b) (c)

(d) (e) (f)

Figure 6: Indoor sites *(a - c)* and outdoor scenarios *(d - f)*.

calibration parameters are provided in Table 1. The handheld setup *(a)* is used in different environments to gather test data. The first testing sites are lab environments as they provide at least two clean and perpendicular walls which are expected to be easy to extract as planes. Since the labs are only normal-sized rooms a wider lobby-like location is added to the dataset. Furthermore, outdoor data is collected between two vans on a parking lot, in front of a building, and in a corner between a building and an overseas container. These sites were chosen because of their use-case-related nature. The different indoor testing sites can be seen in Figures 6a-6c and the outdoor sites are depicted in Figures 6d-6f. The data for setups *(b)* and *(c)* is gathered only in the lab shown in Figure 6b. To compare the findings to the state-of-the-art a calibration using a target similar to (Domhof et al., 2019) and the optimization method of (Peršić et al., 2019) is implemented and extended by an internal offset parameter optimization.

5 RESULTS

For each of the experimental setups, the calibration is estimated 50 times on a recorded data set to test accuracy and reliability. In each setup, the same set of pa-

Table 1: Ground truth and initial calibration parameters for all setups.

		$t_x[m]$	$t_y[m]$	$t_z[m]$	$o[m]$	$r_r[^\circ]$	$r_p[^\circ]$	$r_y[^\circ]$
Ground Truth	Handheld (a)	0.0	0.0	0.095	0.175	0.0	0.0	-145.6
	UAV (b)	0.0	0.0	0.095	0.175	0.0	0.0	0.0
	UGV (c)	0.371	-0.006	-0.402	0.409	0.00	0.01	0.01
Initial	Handheld (a)	0.0	0.0	0.0	0.0	0.0	0.0	-132.0
	UAV (b)	0.0	0.0	0.0	0.0	0.0	0.0	0.0
	UGV (c)	0.3	0.0	-0.5	0.0	0.0	0.0	0.0

Table 2: Mean and standard deviation of estimated parameters ($n = 50$) in all calibration scenarios.

		$t_x[m]$	$t_y[m]$	$t_z[m]$	$o[m]$	$R_{yaw}[^\circ]$	$R_{pitch}[^\circ]$	$R_{roll}[^\circ]$
Lab 1	μ	-0.005	-0.005	0.074	-0.19	-143.275	-0.741	0.927
	σ	0.03	0.034	0.045	0.018	0.942	2.134	1.794
Lab 2	μ	0.014	-0.018	0.089	-0.246	-142.508	0.109	1.357
	σ	0.046	0.038	0.05	0.032	1.449	1.871	1.445
Lobby	μ	0.017	-0.002	0.075	-0.215	-143.707	-6.294	5.518
	σ	0.035	0.037	0.09	0.016	0.713	3.424	2.924
Parked Cars	μ	-0.01	-0.067	0.072	-0.124	-146.099	-2.833	3.752
	σ	0.056	0.066	0.203	0.032	2.055	9.618	8.593
1 Wall	μ	0.003	-0.009	0.032	-0.181	-143.104	1.837	0.677
	σ	0.035	0.041	0.127	0.019	0.702	4.237	3.965
2 Walls	μ	-0.005	-0.002	0.05	-0.168	-146.177	-0.042	-0.056
	σ	0.021	0.022	0.061	0.013	0.427	1.253	1.389
UAV	μ	0.008	0.0	0.142	-0.27	-3.568	-1.274	-0.259
	σ	0.014	0.019	0.052	0.015	0.536	1.79	1.5
UGV	μ	0.325	0.033	-0.148	-0.569	0.888	2.998	-1.836
	σ	0.032	0.064	0.32	0.025	0.519	3.503	7.239

Table 3: Mean estimated parameter uncertainty ($n = 50$) of all calibration scenarios.

	$t_x[m]$	$t_y[m]$	$t_z[m]$	$o[m]$	$R_{yaw}[^\circ]$	$R_{pitch}[^\circ]$	$R_{roll}[^\circ]$
Lab 1	0.127	0.116	0.192	0.105	0.983	2.607	2.323
Lab 2	0.124	0.113	0.172	0.094	1.377	1.972	2.174
Lobby	0.073	0.068	0.128	0.06	0.232	0.597	0.563
Parked Cars	0.121	0.105	0.258	0.098	0.586	1.337	2.617
1 Wall	0.072	0.064	0.187	0.064	0.13	0.702	0.659
2 Walls	0.08	0.091	0.181	0.07	0.56	1.87	1.913
UAV	0.117	0.136	0.209	0.095	1.721	3.242	3.071
UGV	0.089	0.091	0.506	0.081	0.549	3.429	3.757

Table 4: Absolute calibration errors for state-of-the-art and our method (means).

Method	$e_{t_x}[m]$	$e_{t_y}[m]$	$e_{t_z}[m]$	$e_{r_r}[^\circ]$	$e_{r_p}[^\circ]$	$e_{r_y}[^\circ]$	$e_o[m]$
Peršić et al.	0.031	0.009	0.078	0.005	0.012	0.004	0.11
Ours *(Handheld, best)*	0.003	0.002	0.005	0.056	0.042	0.577	0.006
Ours *(Handheld, worst)*	0.017	0.067	0.063	5.518	6.294	3.092	0.071
Ours *(UAV)*	0.008	0.0	0.047	0.259	1.274	3.568	0.1
Ours *(UGV)*	0.046	0.039	0.254	1.836	2.988	0.007	0.16

rameters for the input filtering as well as for matching and binning consisting of three azimuth times three elevation bins ($< -6^\circ, [-6^\circ, 6^\circ), \geq 6^\circ$) is used. Per bin, $N = 15$ plane-to-line matches are extracted for optimization. The only difference between the experiments is the initial calibration which has to match the individual sensor setup and is determined by manual measurement. Table 1 provides the initial parameters. For each optimization, the estimated per-parameter uncertainty is extracted by calculating the

standard deviation from the information matrix used in the graph optimization.

Table 2 shows the mean and the measured standard deviation of the estimated calibration parameters. Independent of the scenario rotational parameters are estimated within a narrow region around ground truth with the only exception being the lobby data set. The same applies to XY-translation and the internal offset parameter. The measured per-parameter standard deviation over all calibration runs shows that most results lie in a region around the mean value of 3 cm to 5 cm or 2°to 4°respectively. Only Z-translation shows a wide range of optimization results. This is expectable for the chosen sensor setups: Z-estimation improves only with high angles of the extracted planes in the lidar data. Using only 16 vertical scans, a heavily tilted plane produces a sparser point cloud which makes plane estimation less reliable compared to a perpendicular plane. This can easily lead to a sparse set of constraints or erroneous plane extractions and could be the reason for the slightly worse calibration results of XY-rotation parameters in the lobby data set. The outdoor data suggests that using two parked cars as calibration targets is a more difficult scenario. Despite good detectability of the metal surfaces in radar data, the plane detection in lidar data gets distorted through the non-optimal shape of the vehicle which leads to a higher deviation in almost all parameters. However, using one or two walls as calibration features produces accurate results, except for the problematic Z-translation, which suggests applicability in the target scenario.

Applicability is also the motivation for the experiments with the UAV and UGV platforms. Using the UAV platform, two operators are able to perform calibration by carrying the robot while rotating and displacing it in front of the calibration features. Gathering all the necessary samples takes less than five minutes additional to the three minutes of optimization runtime on a current laptop CPU.

Since free movement in 6-DOF space is not possible for every sensor setup or robotic application (e.g. think about autonomous driving), an additional experiment is conducted with a UGV platform. By using ramps to ensure at least a limited rotation around the X- and Y-axis, the binning parameters from before can not be used. Instead, five azimuth bins and no elevation binning are configured. The results show that the accuracy in most parameters suffers without the necessary constraints in elevation. Especially rotation estimation around the X- and Y-axis gets more inaccurate with a standard deviation of up to 7°. The greatest discrepancies can be seen in Z-translation with a standard deviation around 0.3 m. Partly these discrepancies can be explained by the lower range resolution of the Navtech radar sensor of 0.06 m but this experiment shows the necessity of the 6-DOF movement for this calibration method.

Another important measure is the uncertainty estimation of the optimization process. Table 3 shows the estimated per-parameter uncertainty for all calibration scenarios. For all translational parameters, this estimation exceeds the actual standard deviations while this is not the case for all the rotation uncertainties. This shows that the assumed error model is not accurate enough to estimate the uncertainty precisely. For example, the error stemming from plane estimation is not modeled in the uncertainty estimation.

To compare the proposed method with the current state-of-the-art target-based method of (Peršić et al., 2017) the UGV sensor setup is used for data acquisition. It is not necessary to move the sensor setup since the calibration target is moved instead. Therefore, the aforementioned problems are not relevant to this experiment. Table 4 lists the absolute calibration error for all experiments. For the comparison, the mean parameter values of the proposed method are used to determine the error. Data shows that the target-less method can compete with the state-of-the-art target-based method or in the best case even outperform it. All the more, when looking at the worst-case absolute errors similar accuracy in translation and intrinsic offset is achieved. Only rotation around the X- and Y-axis are less accurate, although both worst-case estimations stem from the indoor lobby data set. Overall, using the target-less method results in more accurate translation parameters whereas rotation is better estimated by the target-based method.

6 CONCLUSION AND FUTURE WORK

Search and rescue robotics demands techniques that are easily applicable in the field without the need for additional hardware or high-precision equipment. This work shows that it is possible to successfully calibrate a 3D lidar to a 2D scanning radar by only using geometrical features from the environment. An acceptable accuracy regarding absolute calibration error which mostly lies within the discretization accuracy of the radar sensors can be achieved. Only translation along the Z-axis is not estimated well enough. Besides the Z-axis-aligned sensor setup, plane extraction accuracy has a major impact on the optimization of that parameter. In such a setup, only heavily tilted planes introduce the necessary constraints to better es-

timate the Z-translation. In comparison to the state-of-the-art, the proposed method achieves comparable results while not using any artificial calibration targets. This makes the method versatile and applicable in search and rescue scenarios.

In the future, one goal will be the reduction of erroneous plane extractions which add inconclusive constraints to the optimization process. Reducing such mismatches directly improves the parameter estimation and also has a positive effect on the repeatable accuracy. Additional error modeling of the plane extraction process will also improve uncertainty estimation. Furthermore, using bins not only for azimuth and elevation but also for the distance of the plane-line-matches could be beneficial for the optimization result.

ACKNOWLEDGEMENTS

This work has partly been funded by the German Federal Ministry of Education and Research (BMBF) under the project number 13N15550 (UAV-Rescue).

REFERENCES

Domhof, J., Kooij, J. F., and Gavrila, D. M. (2021). A Joint Extrinsic Calibration Tool for Radar, Camera and Lidar. *IEEE Transactions on Intelligent Vehicles*, 6(3):571–582.

Domhof, J., Kooij, J. F. P., and Gavrila, D. M. (2019). A multi-sensor extrinsic calibration tool for lidar , camera and radar. *IEEE International Conference on Robotics and Automation (ICRA)*, pages 1–7.

El Natour, G., Ait-Aider, O., Rouveure, R., Berry, F., and Faure, P. (2015). Toward 3D reconstruction of outdoor scenes using an MMW radar and a monocular vision sensor. *Sensors (Switzerland)*, 15(10):25937–25967.

Fan, H., Bennetts, V. H., Schaffernicht, E., and Lilienthal, A. J. (2019). Towards gas discrimination and mapping in emergency response scenarios using a mobile robot with an electronic nose. *Sensors (Switzerland)*, 19(3).

Fischler, M. a. and Bolles, R. C. (1981). Random Sample Consensus: A Paradigm for Model Fitting with Applications to Image Analysis and Automated Cartography. *Communications of the ACM*, 24(6):381–395.

Fritsche, P., Kueppers, S., Briese, G., and Wagner, B. (2016). Radar and LiDAR Sensorfusion in Low Visibility Environments. In *Proceedings of the 13th International Conference on Informatics in Control, Automation and Robotics (ICINCO)*, volume 2, pages 30–36. SciTePress.

Fritsche, P., Zeise, B., Hemme, P., and Wagner, B. (2017). Fusion of radar, LiDAR and thermal information for hazard detection in low visibility environments. *SSRR 2017 - 15th IEEE International Symposium on Safety, Security and Rescue Robotics, Conference*, pages 96–101.

Heng, L. (2020). Automatic targetless extrinsic calibration of multiple 3D LiDARs and radars. In *IEEE International Conference on Intelligent Robots and Systems*.

Keel, B. M. (2010). Constant False Alarm Rate Detectors. In Richards, M. A., Scheer, J. A., and Holm, W. A., editors, *Principles of Modern Radar: Basic principles*, chapter 16, pages 589–621. Institution of Engineering and Technology, Edison, NJ.

Kim, J. H., Starr, J. W., and Lattimer, B. Y. (2015). Firefighting Robot Stereo Infrared Vision and Radar Sensor Fusion for Imaging through Smoke. *Fire Technology*, 51(4):823–845.

Kummerle, R., Grisetti, G., Strasdat, H., Konolige, K., and Burgard, W. (2011). G2o: A general framework for graph optimization. In *2011 IEEE International Conference on Robotics and Automation*, pages 3607–3613. IEEE.

Peršić, J., Marković, I., and Petrović, I. (2017). Extrinsic 6DoF calibration of 3D LiDAR and radar. *2017 European Conference on Mobile Robots, ECMR 2017*.

Peršić, J., Marković, I., and Petrović, I. (2019). Extrinsic 6DoF calibration of a radar–LiDAR–camera system enhanced by radar cross section estimates evaluation. *Robotics and Autonomous Systems*, 114:217–230.

Peršić, J., Petrović, L., Marković, I., and Petrović, I. (2021). Online multi-sensor calibration based on moving object tracking. *Advanced Robotics*, 35(3-4):130–140.

Scholler, C., Schnettler, M., Krammer, A., Hinz, G., Bakovic, M., Guzet, M., and Knoll, A. (2019). Targetless Rotational Auto-Calibration of Radar and Camera for Intelligent Transportation Systems. In *2019 IEEE Intelligent Transportation Systems Conference (ITSC)*, pages 3934–3941. IEEE.

Sugimoto, S., Tateda, H., Takahashi, H., and Okutomi, M. (2004). Obstacle detection using millimeter-wave radar and its visualization on image sequence. *Proceedings - International Conference on Pattern Recognition*, 3(May):342–345.

Wang, T., Zheng, N., Xin, J., and Ma, Z. (2011). Integrating millimeter wave radar with a monocular vision sensor for on-road obstacle detection applications. *Sensors*, 11(9):8992–9008.

Wise, E., Persic, J., Grebe, C., Petrovic, I., and Kelly, J. (2021). A Continuous-Time Approach for 3D Radar-to-Camera Extrinsic Calibration. In *2021 IEEE International Conference on Robotics and Automation (ICRA)*, pages 13164–13170. IEEE.